Direct magnetocaloric characterization and simulation of thermomagnetic cycles

G. Porcari,[1,2,a)] M. Buzzi,[1,b)] F. Cugini,[1] R. Pellicelli,[1] C. Pernechele,[1] L. Caron,[2] E. Brück,[2] and M. Solzi[1]

[1]*Department of Physics and Earth Sciences, University of Parma, Viale G.P. Usberti n.7/A (Parco Area delle Scienze), 43124 Parma, Italy*

[2]*Fundamental Aspects of Materials and Energy (FAME), Faculty of Applied Sciences, Delft University of Technology, Mekelweg 15, 2629 JB Delft, The Netherlands*

(Received 12 April 2013; accepted 1 July 2013; published online 29 July 2013)

An experimental setup for the direct measurement of the magnetocaloric effect capable of simulating high frequency magnetothermal cycles on laboratory-scale samples is described. The study of the magnetocaloric properties of working materials under operative conditions is fundamental for the development of innovative devices. Frequency and time dependent characterization can provide essential information on intrinsic features such as magnetic field induced fatigue in materials undergoing first order magnetic phase transitions. A full characterization of the adiabatic temperature change performed for a sample of Gadolinium across its Curie transition shows the good agreement between our results and literature data and in-field differential scanning calorimetry. © *2013 AIP Publishing LLC*. [http://dx.doi.org/10.1063/1.4815825]

I. INTRODUCTION

Recently, concern over limited energy resources has driven scientists to explore new, more efficient, and environmentally friendlier energy conversion processes and devices. In this context, energy conversion machines based on the magnetocaloric effect (MCE) represent one of the most promising areas to be developed.[1–4]

The MCE is the entropy or temperature variation in isothermal or adiabatic conditions, respectively, resulting from the perturbation of the system due to the action of a magnetic field.[2,5] The MCE is maximum across magnetic critical processes such as second and especially first order magnetic phase transitions.[6–9] Devices making use of the MCE around phase transitions, must therefore be designed considering the effects of first order transformations. The applicability of even the most promising working material is still constrained by unsolved issues. Reduction of the intrinsic hysteresis due to first order magnetic phase transitions, the minimization of induced structural fatigue due to continuous magnetic field cycling, and a better understanding of the interplay between thermal transport properties and the MCE still pose design challenges.[10–15]

Therefore, the need for novel thermal devices has been continuously pushing scientists to carefully analyze the thermal behavior of magnetic critical processes. During the last years the realization of several in-field calorimetric techniques[16–29] contributed both to a better understanding of the thermomagnetic behavior of the most promising compounds showing first order phase transitions and to encourage the development of new materials.[15,30]

Thus, the study of the time and frequency dependence of the MCE constitutes the next step to be taken.

This means that beyond a complete thermomagnetic characterization (i.e., comparing $c_p(T, H)$, $\Delta s_T(T, \Delta H)$, and $\Delta T_{ad}(T, \Delta H)$ values measured using different calorimetric techniques as well as magnetometry),[28,29,31,32] the analysis of the MCE under operating conditions is essential to bridge material science and device engineering. Such technique should provide insightful information on the impact of fatigue effects and thermal transport-properties on MCE materials.

In the present work, we describe an innovative experimental setup to study the MCE of laboratory-scale samples capable of simulating operating conditions. This technique, based on an adiabatic temperature-change probe, allows high frequency thermomagnetic cycling of systems with mass values ranging between 10^{-2} g and 10^{-1} g. The capabilities as well as the mass sensitivity of the ΔT_{ad} probe are described. This feature, which is seldom reported, together with the comparison of the directly measured MCE data with in-field differential scanning calorimetry (DSC) show the performance of this instrument.

II. EXPERIMENTAL SETUP

The direct measurement of the magnetocaloric temperature-change must be performed under adiabatic conditions: this can be done in different ways. The most common way is to guarantee adiabaticity by changing the magnetic field fast enough so that no considerable thermal exchange can occur. Fast sweeps (10^{-2} s-10^{-1} s) are intrinsic of pulsed fields,[33] while slower ones (10^{-1} s-10^{0} s) are performed mechanically moving the probe or the magnet[31,34–39] or by switching on and off an electromagnet.[33,40–45] The typical sensors used to measure the temperature-change itself are thermocouples[31,33,35,37–42,44,45] or high precision thermoresistances with weak magnetic field dependence.[34,36,43]

a)Electronic mail: giacomo.porcari@fis.unipr.it and G.Porcari@tudelft.nl

b)Present address: Swiss Light Source, Paul Scherrer Institut, CH-5232 Villigen, Switzerland.

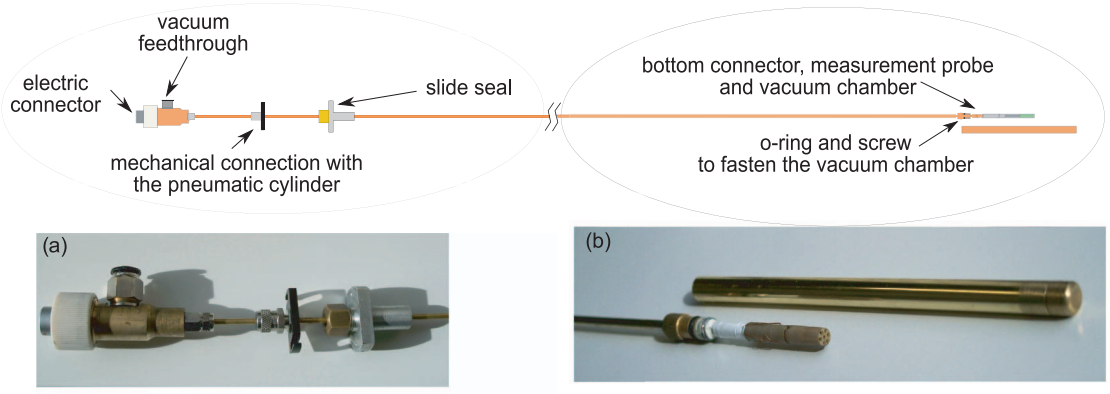

FIG. 1. Sketch of the measurement probe. Panel (a) Top feedthrough, clip assembly, and slide seal, panel (b) lower connector and vacuum chamber.

The experimental setup described here is built to fit different cryostats and to simplify the procedure of sample change, a similar idea was proposed in Ref. 46.

We have designed and realized a measurement probe equipped with 10 electrical connections and a vacuum chamber able to work in pressures of 10^{-4} mbar (see Fig. 1). The wiring was carefully arranged in twisted pairs to reduce the inductive voltage pickup due to the variable magnetic field as much as possible. The body was built from a 3 mm seamless brass tube while on the top a purpose-designed feedthrough decouples the electric connector (Fischer DBEE model) from the pumping system (Fig. 1(a)). The vacuum chamber (external diameter ϕ7 mm) can be attached to the bottom end of the probe through a screw. The reduced dimensions allow the use of this probe in MPMS® Quantum Design cryostats. Epoxy resin able to work at low temperatures is used to secure the lower connector (a 7 pin Fischer) to the main body (Fig. 1(b)). The slide seal assembly shown in Figure 1(a) is a modified version of the original one by Quantum Design. While its dimensions are the same, a mechanical constraint is added inside to prevent the o-rings from getting loose during the fast insertion of the probe in the magnetic field region. An additional flange is needed to fit this probe in different cryostats with a KF inlet.

A. Adiabatic temperature-change probe

The heart of the probe is the thermoresistance and the sample housing (Fig. 2(a)). A Cernox™ bare chip characterized by a mass of 3 mg and time response of 0.135 s is used to measure the sample temperature.[47] Its magnetoresistance has been reported to be significant just at low temperatures and in high applied magnetic fields.[25,48,49] The Cernox™ is glued using epoxy resin on a fiberglass board equipped with gold contacts to preserve it from mechanical stresses (Fig. 2(b)). The gold bonding is made through thermocompression directly on the bare chip (Fig. 2(b)). The fiberglass board is fixed in a PEEK housing, while the sensor chip is put downwards to protect the wires (Fig. 2(a)). A cavity in the PEEK avoids any contact between the Cernox™ chip surface and the probe. The external diameter of the sample holder is 4.5 mm while its housing size (respectively, width and depth) is 3 × 2 mm. The sample is in contact with the back side of the Cernox™ through a thermoconductive paste (Arctic Ceramique $k \sim 7$ W m^{-1} K^{-1}). The sample is then glued in two points on the fiberglass with GE-Varnish to minimize heat losses through the probe. The Cernox™ is powered by an ac current of a few μA at 1 kHz and its voltage signal is filtered by a lock-in amplifier whose time constant is set to 10 ms.

In the preliminary experiments, the adiabatic temperature-change characterization is performed turning on and off a low inductive electromagnet while the probe does not move. The magnetic field sweep rate is detected by a solenoid placed between the poles (Fig. 3(a)). The peak value of the external field ($\mu_0 H = 1.92 \pm 0.05$ T) is measured by a Lakeshore 460 3-channel Hall effect gaussmeter. It can be seen (Fig. 3(a)) that the magnetic field reaches 95% of its maximum value in 1 s, while the average field sweep rate turns out to be 1.8 T s^{-1}. The temperature in this case is controlled by means of a continuous flow cryostat (purchased from "Très Basses Températures - TBT" group Air Liquide).

B. Brayton thermomagnetic cycles setup

The described probe can be used to simulate thermomagnetic cycles consisting of two adiabatic and two isofield

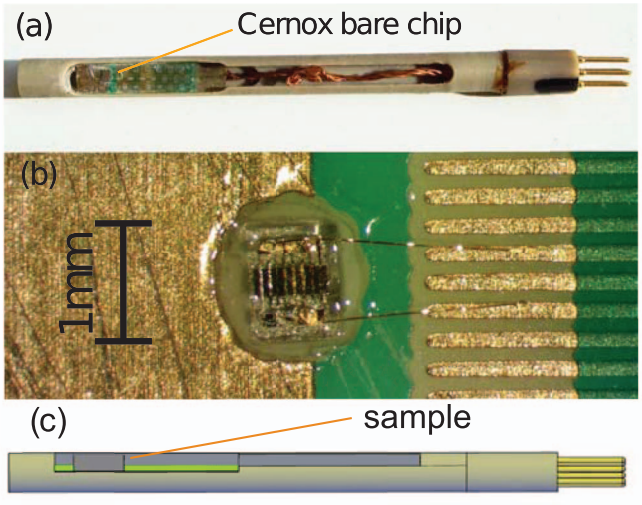

FIG. 2. (a) Adiabatic temperature-change probe, (b) Cernox™ bare chip glued on the supporting plate, (c) sketch of the adiabatic temperature-change probe with sample.

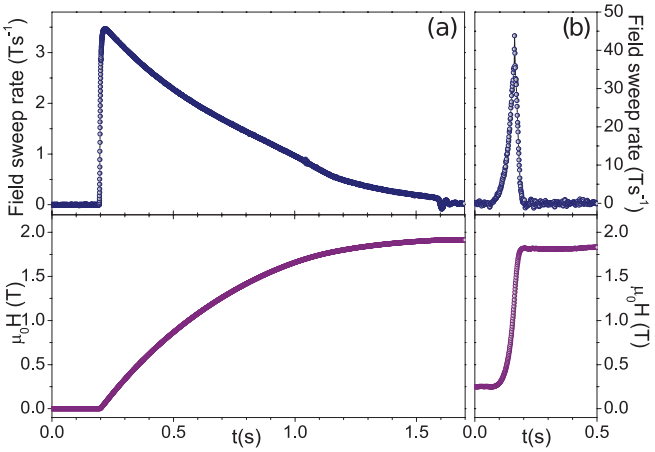

FIG. 3. Temporal evolution of the magnetic field and effective sweep rate for the two cases: (a) the electromagnet is turned on, (b) the pneumatic actuator places the sample in the high field region of the magnet.

branches. A pneumatic cylinder is then used to insert and extract the sample in and out of the magnetic field. The cylinder "running" time is about 0.15 s (see Fig. 3(b)) while the average magnetic field sweep rate is $\mu_0 dH/dt = 10$ T s^{-1}. Note that in these conditions the working limit of this temperature sensor is approached since its time response is 135 ms while the magnetic field sweeps in about 150 ms. The cryostat is a continuous flow Oxford Instruments CF1200 while the magnetic field source is an electromagnet whose maximum magnetic field is 1.85 T. The simulated Brayton cycle consists of two stages at different magnetic field and temperature. To accurately control the temperature in the out-of-field region (outside the sample space), a cryostat insert has been designed and realized (Fig. 4). The insert is a tube made of two copper regions (one between the poles of the electromagnet and the other outside) thermally insulated one from the other using a Tufnol® section (Fig. 4). The temperature at which the sample is extracted and inserted is changed through two Omega Kapton Insulated Flexible Heaters able to power up to 20 W.[50] Different cycling frequencies can be achieved controlling the temperatures of the two field regions and the relaxation rates. In these experiments, the vacuum chamber is not used and the sample is directly exposed to the heat exchange medium which is helium gas. In this configuration, however, helium is not flowing through the sample space and it helps the system to relax to the outer temperature mainly through conduction. Thermal radiation between the probe and the surrounding walls also plays a not negligible role on the temperature profile during the isofield branches. The main difference with real applications is then that we do not exchange heat through convection with a flowing fluid.

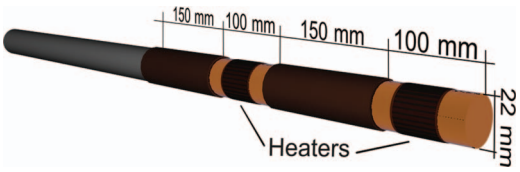

FIG. 4. Drawing of the cryostat insert. This attachment allows to control the system temperature in the zero field region.

III. RESULTS AND DISCUSSION

A. Direct adiabatic temperature-change measurement

The material used to test the present setup was a Goodfellow 99.9% pure Gadolinium plate. The Cernox™ bare chip is mainly made of sapphire.[47] Its mass ($m_{Cx} = 3$ mg) takes into account not only the substrate but also the gold plating, contacts and film itself. The Cernox™ heat capacity at room temperature can be estimated at about 1 mJ K^{-1}, which is comparable to that of a Gadolinium sample of 3.5 mg (considering $c_{pGd} = 300$ J kg^{-1} K^{-1} across its Curie temperature). When studying the MCE of small samples, the balance between their heat capacity and that of the sensor cannot be neglected. This effect, which leads to measure a ΔT_{ad} lower than what is experienced by the material, is systematic so it can be taken into account if the specific heat of the sample is known. A simple proportion allows to estimate the size of this effect

$$\Delta T_{ad_{Gd}}(T) = \Delta T_{ad_{Cx}}(T)\frac{m_{Cx}c_{pCx}(T) + m_{Gd}c_{pGd}(T)}{m_{Gd}c_{pGd}(T)}, \quad (1)$$

where $\Delta T_{ad_{Gd}}(T)$ is the effective adiabatic temperature-change experienced by the sample due to the action of the field, while $\Delta T_{ad_{Cx}}(T)$ is the temperature variation of the sensor which is what we are actually measuring. Then in Eq. (1), $c_{pCx}(T)$ is the Cernox™ specific heat and m_{Gd} is the Gadolinium sample mass. This equation allows the correction of the measured $\Delta T_{ad_{Cx}}$ values for low heat capacity systems. The Gadolinium specific heat value $c_{pGd}(T)$ in this branch is an average between the in-field and the zero field specific heat curves which were directly measured by means of a home made in-field differential scanning calorimeter.

The studied Gadolinium sample is chosen large enough (110 mg) to minimize this effect. Its magnetocaloric adiabatic behavior for a field span of $\mu_0\Delta H = 1.65$ T is shown in Figure 5. In this graph, the regions where the magnetic field is turned on (heating) and off (cooling) are shown. The measurement error (±0.15 K) is due to the sensor electric noise and corresponds to a resistance resolution of ±0.01 Ω.[29,51] The shape of the relaxation branch (after the temperature peak) reported in Figure 5 reflects non-ideal adiabatic conditions: this effect on the obtained data is discussed subsequently. The magnetic field profile (corresponding to Fig. 3(a)) superimposed to the acquired temperature data is zoomed in in the inset of Figure 5: its vertical axis is rescaled on the expected ΔT_{ad} value deduced on the basis of in-field DSC data. This profile thus describes the expected temperature vs. time measurement profile. This comparison shows that the shape of the curve at the transition depends on the magnetic field profile rather than on non-ideal adiabatic conditions. This inset also shows the temperature data obtained when taking into account the thermoresistance heat capacity (Eq. (1)). The correction in this case is less than 2.5% of the measured peak value. The data reported hereinafter have been corrected.

The magnetic field dependence of the MCE measured at the temperature of maximal response (292 K) is displayed in Figure 6. The horizontal axis is the internal field, which is calculated from a demagnetizing factor of N = 0.3 along the measurement direction. It is worth noticing that this is required for a proper comparison with literature data.[31,32,52,53]

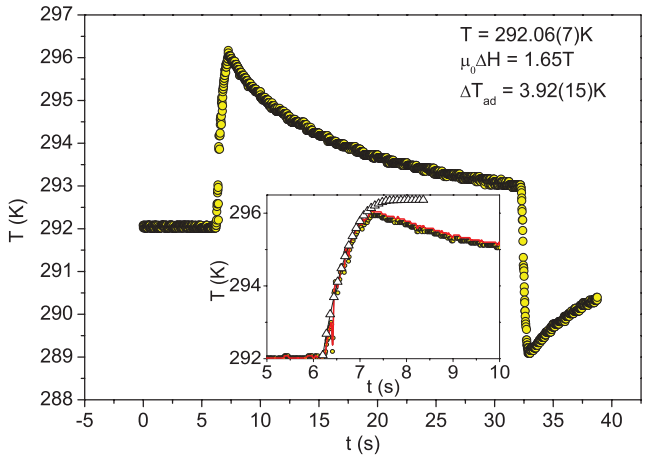

FIG. 5. Direct ΔT_{ad} measurement across the Curie temperature of a Gadolinium sample in $\mu_0 \Delta H = 1.65$ T both switching the field on and off. (Inset) Superimposed magnetic field profile (white triangles) normalized on the maximum expected ΔT_{ad} and the temperature profile obtained taking into account the sensor heat capacity (red thin profile). Yellow circles are the raw data.

The inset shows the MCE as function of $(\mu_0 H)^{2/3}$: the slope of this curve ($A = 3.02 \pm 0.03$ KT$^{-2/3}$) constitutes a further marker of the material quality.[52]

The temperature behavior of the MCE of the Gadolinium sample for a field sweep of $\mu_0 \Delta H = 1.65$ T is shown in Figure 7. The comparison between the "heating" and the "cooling" $\Delta T_{ad}(T)$ curves does not reveal, at least for these magnetic fields sweeps, any influence of eddy currents as suggested in Ref. 34. Excluding skin effects (the magnetic field is assumed to fully penetrate the sample at these time scales), it can be estimated that the heat produced by eddy currents could contribute about 10^{-2} K, thus falling within the measured $\Delta T_{ad}(T)$ errorbars.

The directly measured ΔT_{ad} values are superimposed in Figure 7 to the estimate of the same quantity derived from in-field DSC. This cross characterization is needed since the MCE of rare earths elements is strongly affected by their degree of purity, thus making it difficult to compare our results

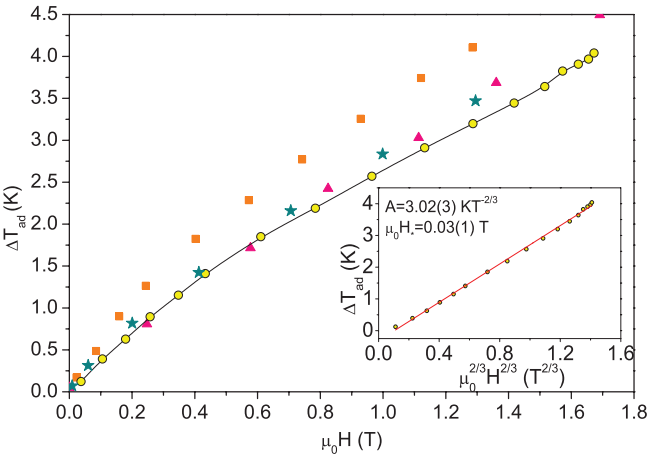

FIG. 6. ΔT_{ad} vs. magnetic field at 292 K. Our characterization (yellow circles) is compared with values shown in Ref. 52 (■ symbol), Ref. 53 (★ symbol), and Ref. 54 (▲ symbol). (Inset) Demonstrates the linear $\mu_0^{2/3} H^{2/3}$ dependence of the ΔT_{ad} curve.

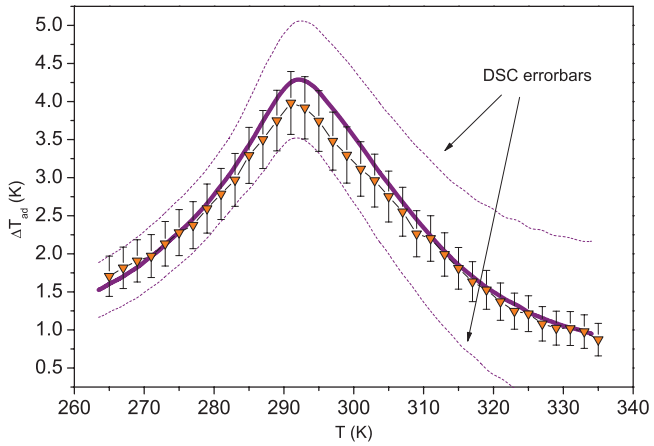

FIG. 7. ΔT_{ad} vs. temperature for magnetic field change of $\mu_0 \Delta H = 1.65$ T (triangles). This measurement is compared with in-field DSC performed on the same sample for a $\mu_0 \Delta H = 1.7$ T field variation (purple line).

with literature data.[54,55] The specifications of the in-field DSC technique are described in Ref. 29. The calorimetric characterization for Gadolinium is performed using a sweep rate of 0.03 K s^{-1} at (internal) magnetic fields of $\mu_0 H_i = 0$ T and $\mu_0 H_f = 1.7$ T. The effective relative error was deduced to be within 0.6%. This is mainly due to slightly unstable vacuum conditions which affect the specific heat baselines of the in-field and zero field temperature scans with different systematic errors.[56] The demagnetizing field is estimated to be 0.3 T for the direct ΔT_{ad} measurements and 0.14 T for the DSC analysis since the sample orientation with respect to the field direction is different in the two cases. Figure 7 clearly shows the good agreement between the outcomes of the two techniques. Looking at the MCE peaks, the direct probe yields $\Delta T_{ad} = 4.04 \pm 0.37$ for a magnetic field span of $\mu_0 \Delta H = 1.65$ T, while from calorimetry $\Delta T_{ad} = 4.29 \pm 0.77$ K is obtained for a magnetic field change of $\mu_0 \Delta H = 1.7$ T. Both techniques are in good agreement within the error. The uncertainty of the direct ΔT_{ad} turns out to be much lower than that of DSC. This point supports the use of a purely adiabatic technique instead of indirect isofield or isothermal methods to obtain a precise estimation of the ΔT_{ad}.[29]

For ideal adiabatic conditions, Eq. (1) gives an exact description of the relation between the adiabatic temperature-change and the measured value. We therefore expect the measured ΔT_{ad} to be a strong function of the sample mass. The latter has been checked by measuring Gd samples of different masses (as displayed in Fig. 8). We also include in Fig. 8 the expected ΔT_{ad} which takes into account the Cernox^{TM} heat capacity as described in Eq. (1). It can be checked how for samples with heat capacities down to 0.03 J K^{-1} heat losses can be neglected. This effect is pronounced across second order transitions, and in case of gadolinium it appears even larger because of its low specific heat.

The curve reported in Figure 8 can thus be considered as the (mass) sensitivity of the described technique for Gadolinium. A more general sensitivity curve is shown in Figure 9 where the temperature-change is normalized to its maximum value. This is useful to compare the mass dependence of the measured ΔT_{ad} for systems with different MCE.

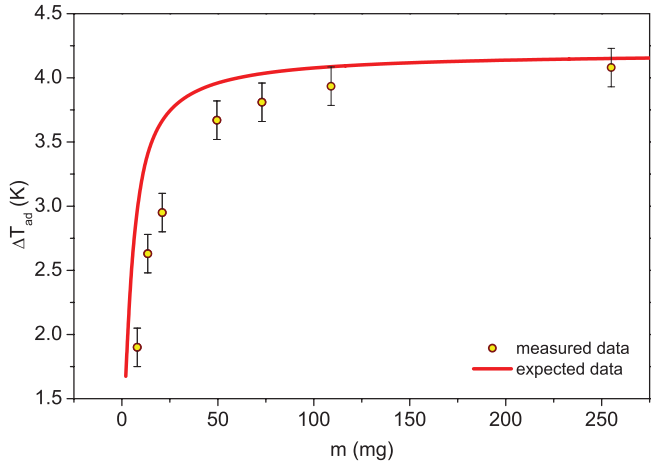

FIG. 8. ΔT_{ad} vs. gadolinium sample mass at 292 K for a magnetic field change $\mu_0 \Delta H = 1.7$ T (circles). The expected ΔT_{ad} as deduced from Eq. (1) (red line).

In this plot, the white circles represent a curve corresponding to the expected ΔT_{ad} peak values across an inverse martensitic transformation of a Ni–Co–Mn–Ga Heusler alloy. Its specific heat behavior is shown in Figure 10. As predicted in this case, the full effect can also be measured on a sample of 30 mg without the need of any correction due to the presence of latent heat (inset of Fig. 10).

Another way to visualize Eq. (1) is drawn in inset of Figure 9. This curve represents the more general sensitivity curve of this technique, which applies to a generic sample as function of the ratio between sample and Cernox^{TM} heat capacities. A similar trend of the expected ΔT_{ad} values has been discussed in Ref. 35 as function of the system diffusivity.

B. Thermomagnetic cycles

The temperature dependence of the entropy of our Gadolinium sample at internal fields of $\mu_0 H = 0.17$ T and $\mu_0 H = 1.65$ T is shown in Figure 11.

The specific heat profiles at $\mu_0 H \sim 0$ T, $\mu_0 H = 0.17$ T, and $\mu_0 H = 1.65$ T are reported in the inset. Here, our DSC measurements are compared with data obtained from

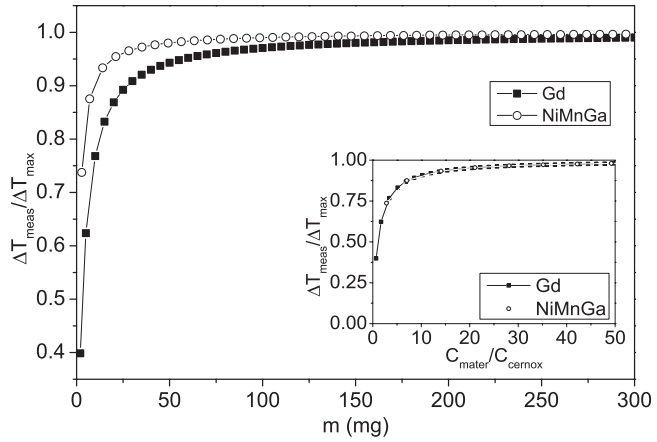

FIG. 9. Relative $\Delta T_{ad_{Cx}} / \Delta T_{ad_{sample}}$ vs. mass for Gadolinium (black) and $Ni_{45}Co_5Mn_{30}Ga_{20}$ Heusler (white). (Inset) Normalized ΔT_{ad} vs. sample/sensor heat capacity ratio. These curves describe the sensitivity of the ΔT_{ad} probe.

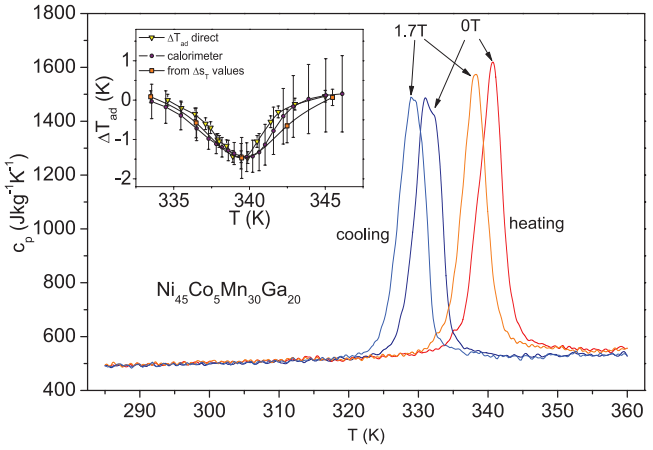

FIG. 10. Specific heat and MCE (in inset) as measured on a 30 mg piece $Ni_{45}Co_5Mn_{30}Ga_{20}$ Heusler alloy for $\mu_0 \Delta H = 1.7$ T.

Ref. 54. Looking at the zero-field measurements it can be noticed how the specific heat curves for the two commercial polycrystalline samples are in good agreement (our c_p errorbar is estimated to be within 3%) while the effect of impurities can be appreciated from the difference with the c_p profile of the single crystal. The specific heat curve at 0.17 T shows then how the effect of a relatively weak applied field broadens considerably the measurement made in zero-field.

This temperature and magnetic field dependence is used to obtain the ΔT_{ad} calorimetric profile in the curve of Figure 7 (however with the low field curve measured at 0 T). As an example of a simple thermomagnetic cycle, we include in this entropy-temperature diagram the loop that the system will follow during the direct measurement experiment. The cycle of Figure 11 consists of two adiabatic and two isofield branches thus reproducing an idealized Brayton cycle.[2]

In Figure 12, we show four different thermomagnetic cycles performed on the Gadolinium sample of 110 mg near its Curie temperature for different hot and cold cycle temperatures (T_h and T_c) and frequencies. T_h and T_c are the set points at which the sample is extracted and inserted from and in the magnetic field, respectively. The frequency of the

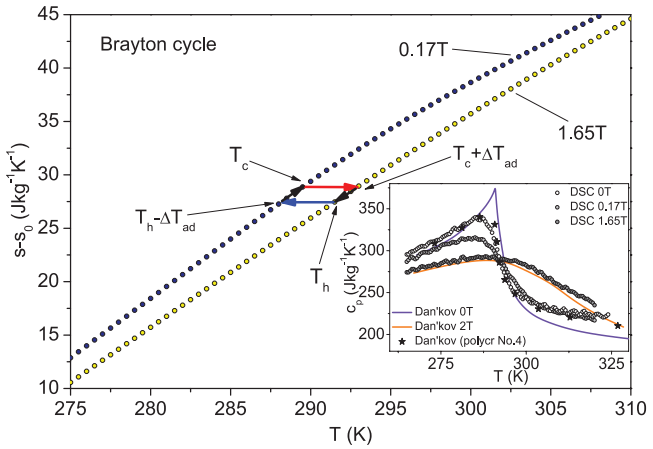

FIG. 11. Temperature dependence of entropy in $\mu_0 H = 0.17$ T and $\mu_0 H = 1.65$ T. The thermomagnetic cycle of Figure 12(b) is shown. (Inset) c_p curves compared with data from Ref. 54.

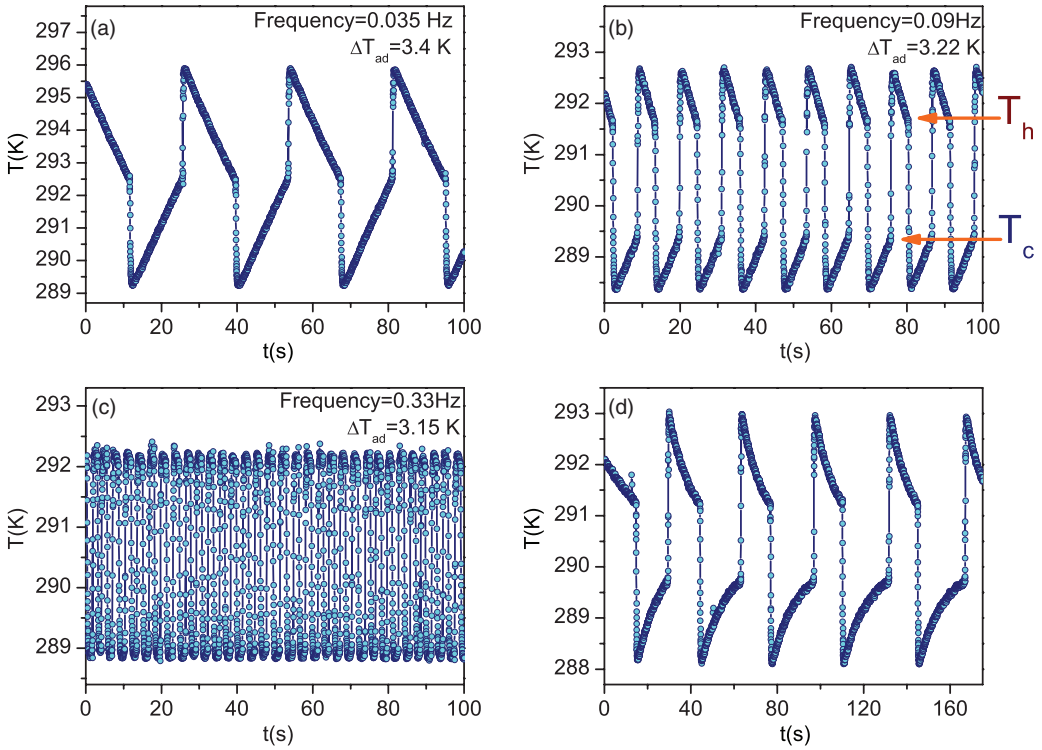

FIG. 12. Thermomagnetic cycles derived from direct ΔT_{ad} characterization at different frequencies. Figures (a)–(c) show the Gadolinium magnetocaloric behavior for different T_h and T_c temperatures of the cycle. Figure (d) shows the system temperature relaxation for a controlled asymmetric background temperature.

thermomagnetic cycles is a function of both the relative position of T_h and T_c as well as the temperatures of the in-field ($\mu_0 H = 1.65$ T) and out-of-field ($\mu_0 H = 0.17$ T) regions which affects the relaxation rate of the isofield branches.

The reproducibility of the effect on subsequent branches for every experiment is striking. The absence of hysteresis is verified since no differences are observed comparing the first ΔT_{ad} branch and the following ones. The effective internal field change is: $\mu_0 \Delta H \sim 1.5$ T.

The measured $\Delta T_{ad} = 3.4 \pm 0.35$ K at 292.5 K (panel (a)) turns out to be in agreement with both the values of Figure 6 and with the calorimetric estimation of 3.54 ± 0.72 K. This result shows the reliability of the Cernox™ sensor also at the sweep rate utilized with this setup.

To increase the operational frequency up to 0.33 Hz, a faster thermal relaxation was needed (panels (b) and (c)). In these two cases (referring to the MCE induced by increasing field), the measured ΔT_{ad} is 3.22 K and 3.15 K at 289.5 K and 289 K while the DSC ΔT_{ad} estimations for the same temperatures are 3.42 ± 0.63 K and 3.38 ± 0.62 K, corresponding to a 6% deviation from the expected values. This result also shows the good instrument operation at relatively high thermal relaxation rates. In Figure 12(d), while performing the measurement, the temperature of the out-of-field region was changed in order to show how the non-ideal adiabaticity of the isofield branches can be controlled depending on the heater power. This feature allows to adequately change the cycles time period depending on the particular characterization requirement.

In this setup, the loop frequency can be increased by changing the two controlled temperatures of the cryostat insert shown in Figure 4. In particular for the examples of Figure 12, the in-field region is kept at lower temperatures than the out-of-field one. The system heats up when it is put in the magnetic field but it suddenly starts to cool down. As soon as its temperature equals the "virtual" T_h, the sample is extracted from the field. This setup thus does not constitute an effective magnetic refrigerator.

However, the key point lies in the possibility to analyze the behavior of low mass laboratory-scale samples when exposed to external fields in nearly operative conditions.

As highlighted in recent works, the impact of hysteresis on the magnetocaloric properties of first order materials should always be discussed.[35,57–59] This instrument could give information about the reversibility of magnetic phase transitions as well.

Furthermore, the control of the cycle temperature range, field span, and frequency could help studying fatigue on the material structure induced by application and removal of the magnetic field.

Comparison of the thermomagnetic cycles of materials with different thermal conductivities could show whether different thermal transport properties pose a limit to the maximum achievable cycle frequency.

IV. CONCLUSION

The study of the MCE under operating conditions is necessary to advance both working materials development and prototype design. This is achieved through the performance of realistic thermomagnetic cycles, allowing the time and frequency dependent characterization of the MCE under operating conditions.

The described technique based on an adiabatic temperature-change probe yields results in good agreement with both DSC measurements and values reported in literature. The mass sensitivity of the ΔT_{ad} probe is reported.

In this work, we show the next step towards the complete characterization of MCE materials for applications, addressing the yet overlooked issue of the interplay between thermal conductivity and the MCE as well as fatigue effects. This approach could be insightful in describing processes close to the critical point between first and second order behaviors,[60] shown by the most promising materials for applications.[61–63]

ACKNOWLEDGMENTS

The authors thank Dr. Franca Albertini and Dr. Simone Fabbrici of the Group of "Magnetic Materials" of IMEM-CNR for the provided samples and Dr. Enos Gombia of the Group of "Electrical measurements" of IMEM-CNR for the help offered bonding the gold wires on the Cernox™ bare chip. The authors are also grateful to Alberto Bazzini, former leader of the Physics and Earth Sciences Department mechanical workshop (University of Parma), for the key technical solutions proposed and Dr. Massimiliano Zanichelli of the Group of "Optoelectronics and devices" of Physics and Earth Sciences Department (University of Parma), for fruitful discussion and support.

[1] C. Zimm, A. Jastrab, A. Sternberg, V. Pecharsky, K. Gschneidner, M. Osborne, and I. Anderson, Adv. Cryog. Eng. **43**, 1759 (1998).
[2] A. M. Tishin and Y. I. Spichkin, *The Magnetocaloric Effect and its Applications* (Institute of Physics, Bristol, 2003).
[3] K. Engelbrecht, G. Nellis, and S. Klein, HVAC&R Res. **12**, 1077 (2006).
[4] A. Kitanovski and P. Egolf, Int. J. Refrig. **33**, 449 (2010).
[5] V. K. Pecharsky, K. A. Gschneidner, Jr., A. O. Pecharsky, and A. M. Tishin, Phys. Rev. B **64**, 144406 (2001).
[6] K. A. Gschneidner, Jr., V. K. Pecharsky, and A. O. Tsokol, Rep. Prog. Phys. **68**, 1479 (2005).
[7] A. Smith, C. R. H. Bahl, R. Bjørk, K. Engelbrecht, K. K. Nielsen, and N. Pryds, Adv. Energy Mater. **2**, 1288 (2012).
[8] E. Brück, "Magnetocaloric refrigeration at ambient temperature," in *Handbook of Magnetic Materials*, edited by K. H. J. Buschow (Elsevier, Amsterdam, 2007), Vol. 17, Chap. 4.
[9] V. Franco, J. S. Blázquez, B. Ingale, and A. Conde, Annu. Rev. Mater. Res. **42**, 305 (2012).
[10] O. Gutfleisch, M. A. Willard, E. Brück, C. H. Chen, S. G. Sankar, and J. P. Liu, Adv. Mater. **23**, 821 (2011).
[11] K. A. Gschneidner, Jr. and V. K. Pecharsky, Int. J. Refrig. **31**, 945 (2008).
[12] J. Lyubina, J. Appl. Phys. **109**, 07A902 (2011).
[13] J. Lyubina, U. Hannemann, M. P. Ryan, and L. F. Cohen, Adv. Mater. **24**, 2042 (2012).
[14] R. A. Booth and S. A. Majetich, J. Appl. Phys. **111**, 07A933 (2012).
[15] K. G. Sandeman, Scr. Mater. **67**, 566 (2012).
[16] T. Plackowski, Y. Wang, and A. Junod, Rev. Sci. Instrum. **73**, 2755 (2002).
[17] J. Marcos, F. Casanova, X. Batlle, A. Labarta, A. Planes, and L. Mañosa, Rev. Sci. Instrum. **74**, 4768 (2003).
[18] A. A. Minakov, S. B. Roy, Y. V. Bugoslavsky, and L. F. Cohen, Rev. Sci. Instrum. **76**, 043906 (2005).
[19] L. Tocado, E. Palacios, and R. Burriel, J. Therm. Anal. Calorim. **84**, 213 (2006).
[20] V. Basso, M. Küpferling, C. P. Sasso, and L. Giudici, Rev. Sci. Instrum. **79**, 063907 (2008).
[21] Y. Miyoshi, K. Morrison, J. D. Moore, A. D. Caplin, and L. F. Cohen, Rev. Sci. Instrum. **79**, 074901 (2008).
[22] S. Jeppesen, S. Linderoth, N. Pryds, L. T. Kuhn, and J. B. Jensen, Rev. Sci. Instrum. **79**, 083901 (2008).
[23] J. C. P. Klaasse and E. H. Brück, Rev. Sci. Instrum. **79**, 123906 (2008).
[24] V. Hardy, Y. Breard, and C. Martin, J. Phys.: Condens. Matter **21**, 075403 (2009).
[25] Y. Kohama, C. Marcenat, T. Klein, and M. Jaime, Rev. Sci. Instrum. **81**, 104902 (2010).
[26] V. Basso, C. P. Sasso, and M. Küpferling, Rev. Sci. Instrum. **81**, 113904 (2010).
[27] K. Morrison, M. Bratko, J. Turcaud, A. Berenov, A. D. Caplin, and L. F. Cohen, Rev. Sci. Instrum. **83**, 033901 (2012).
[28] K. Morrison, K. G. Sandeman, L. F. Cohen, C. P. Sasso, V. Basso, A. Barcza, M. Katter, J. D. Moore, K. P. Skokov, and O. Gutfleisch, Int. J. Refrig. **35**, 1528 (2012).
[29] G. Porcari, F. Cugini, S. Fabbrici, C. Pernechele, F. Albertini, M. Buzzi, M. Mangia, and M. Solzi, Phys. Rev. B **86**, 104432 (2012).
[30] K. A. Gschneidner, Jr., Y. Mudryk, and V. K. Pecharsky, Scr. Mater. **67**, 572 (2012).
[31] R. Bjørk, C. R. H. Bahl, and M. Katter, J. Magn. Magn. Mater. **322**, 3882 (2010).
[32] J. D. Moore, K. P. Skokov, J. Liu, and O. Gutfleisch, J. Appl. Phys. **112**, 063920 (2012).
[33] S. Yu. Dankov, A. M. Tishin, V. K. Pecharsky, and K. A. Gschneidner, Rev. Sci. Instrum. **68**, 2432 (1997).
[34] B. R. Gopal, R. Chahine, and T. K. Bose, Rev. Sci. Instrum. **68**, 1818 (1997).
[35] J. Kamarád, J. Kaštil, and Z. Arnold, Rev. Sci. Instrum. **83**, 083902 (2012).
[36] S. Fujieda, Y. Hasegawa, A. Fujita, and K. Fukamichi, J. Magn. Magn. Mater. **272–276**, 2365 (2004).
[37] A. R. Dinesen, S. Linderoth, and S. Mørup, J. Phys.: Condens. Matter **17**, 6257 (2005).
[38] M. P. Annaorazov, S. A. Nikitin, A. L. Tyurin, K. A. Asatryan, and A. Kh. Dovletov, J. Appl. Phys. **79**, 1689 (1996).
[39] J. Liu, T. Gottschall, K. P. Skokov, J. D. Moore, and O. Gutfleisch, Nature Mater. **11**, 620 (2012).
[40] S. M. Benford and V. G. Brown, J. Appl. Phys. **52**, 2110 (1981).
[41] X. Moya, L. Manosa, A. Planes, S. Aksoy, M. Acet, E. F. Wassermann, and T. Krenke, Phys. Rev. B **75**, 184412 (2007).
[42] F. Canepa, S. Cirafici, M. Napoletano, C. Ciccarelli, and C. Belfortini, Solid State Commun. **133**, 241 (2005).
[43] H. Wada, T. Asano, M. Ilyn, and A. M. Tishin, J. Magn. Magn. Mater. **310**, 2811 (2007).
[44] G. C. Lin, C. D. Xu, and J. X. Zhang, J. Magn. Magn. Mater. **283**, 375 (2004).
[45] G. V. Brown, J. Appl. Phys. **47**, 3673 (1976).
[46] B. A. Assaf, T. Cardinal, P. Wei, F. Katmis, J. S. Moodera, and D. Heiman, Rev. Sci. Instrum. **83**, 033904 (2012).
[47] Cernox™ datasheet at http://www.lakeshore.com/Documents/LSTC_Cernox_l.pdf for information about the bare chip.
[48] B. L. Brandt, D. W. Liu, and L. G. Rubin, Rev. Sci. Instrum. **70**, 104 (1999).
[49] J. C. P. Klaasse, I. H. Hagmusa, and E. H. Brück, Rev. Sci. Instrum. **68**, 4208 (1997).
[50] See http://www.omega.com/Heaters/pdf/KHR_KHLV_KH.pdf for information about the Kapton flexible heaters used.
[51] G. Porcari, S. Fabbrici, C. Pernechele, F. Albertini, M. Buzzi, A. Paoluzi, J. Kamarad, Z. Arnold, and M. Solzi, Phys. Rev. B **85**, 024414 (2012).
[52] M. D. Kuz'min, K. P. Skokov, D. Yu. Karpenkov, J. D. Moore, M. Richter, and O. Gutfleisch, Appl. Phys. Lett. **99**, 012501 (2011).
[53] C. R. H. Bahl and K. K. Nielsen, J. Appl. Phys. **105**, 013916 (2009).
[54] S. Yu. Dankov, A. M. Tishin, V. K. Pecharsky, and K. A. Gschneidner, Phys. Rev. B **57**, 3478 (1998).
[55] V. K. Pecharsky and K. A. Gschneidner, Jr., Adv. Cryog. Eng. **42A**, 423 (1996).
[56] V. K. Pecharsky and K. A. Gschneidner, Jr., J. Appl. Phys. **86**, 565 (1999).
[57] K. P. Skokov, V. V. Khovaylo, K. H. Müller, J. D. Moore, J. Liu, and O. Gutfleisch, J. Appl. Phys. **111**, 07A910 (2012).
[58] Ö. Çakır and M. Acet, Appl. Phys. Lett. **100**, 202404 (2012).
[59] I. Titov, M. Acet, M. Farle, D. Gonzalez-Alonso, L. Manosa, A. Planes, and T. Krenke, J. Appl. Phys. **112**, 073914 (2012).
[60] K. Morrison, A. Dupas, Y. Mudryk, V. K. Pecharsky, K. A. Gschneidner, A. D. Caplin, and L. F. Cohen, Phys. Rev. B **87**, 134421 (2013).
[61] K. Morrison, J. Lyubina, J. D. Moore, K. G. Sandeman, O. Gutfleisch, L. F. Cohen, and A. D. Caplin, Philos. Mag. **92**, 292 (2012).
[62] N. H. Dung, L. Zhang, Z. Q. Ou, and E. Brück, Appl. Phys. Lett. **99**, 092511 (2011).
[63] N. H. Dung, Z. Q. Ou, L. Caron, L. Zhang, D. T. C. Thanh, G. A. de Wijs, R. A. de Groot, K. H. J. Buschow, and E. Brück, Adv. Energy Mater. **1**, 1215 (2011).